A: Kinetics, Dynamics, Photochemistry, and Excited States

The Atmospheric Photo-Oxidation of Diethyl Carbonate: Kinetics, Products, and Reaction Mechanism

Guido Noe Rimondino, Walter José Peláez, and Fabio Ernesto Malanca

J. Phys. Chem. A, **Just Accepted Manuscript** • DOI: 10.1021/acs.jpca.9b09887 • Publication Date (Web): 04 Dec 2019

The Atmospheric Photo-Oxidation of Diethyl Carbonate: Kinetics, Products, and Reaction Mechanism

Guido N. Rimondino, Walter J. Peláez, and Fabio E. Malanca*

INFIQC - CONICET - Instituto de Investigaciones en Fisicoquímica de Córdoba. Departamento de Fisicoquímica, Facultad de Ciencias Químicas. Universidad Nacional de Córdoba, Ciudad Universitaria (X5000HUA), Córdoba, República Argentina.

***Corresponding author**

Guido Noé Rimondino

INFIQC - CONICET

Departamento de Fisicoquímica - Facultad de Ciencias Químicas

Universidad Nacional de Córdoba

grimondino@fcq.unc.edu.ar

ABSTRACT

The rate coefficient for the gas-phase of diethyl carbonate with chlorine atoms has been determined at 298 K using a relative method, employing ethyl formate and ethyl acetate as reference compounds. The experimental value, $(1.0 \pm 0.2) \times 10^{-11}$ cm^3 $molecule^{-1}$ s^{-1}, is in good correlation with the one estimated by the SAR (Structure-Activity Relationship) method. The photo-oxidation mechanism of diethyl carbonate initiated by chlorine atoms was also studied at 298 K and atmospheric pressure as a function of the oxygen partial pressure. The main products identified by infrared spectroscopy were: $CH_3CH_2OC(O)OCHO$, $CH_3CH_2OC(O)OCH_2CHO$, $CH_3CH_2OC(O)OC(O)CH_3$, CO_2, CO, HCOOH, and CH_3COOH. The results reveal that the oxidation process occurs by the abstraction of a hydrogen atom from the methyl (43%) and methylene (57%) groups. The relative importance of each reaction path from the primary radicals formed in photo-oxidation and the identity of $CH_3CH_2OC(O)OCHO$, $CH_3CH_2OC(O)OC(O)CH_3$, and $CH_3CH_2OC(O)OCH_2CHO$ were determined using computational methods. The activation energy of reaction paths for the main oxygenated radicals formed during photo-oxidation was determined using Gaussian09 Program.

INTRODUCTION

Diethyl carbonate (DEC, $CH_3CH_2OC(O)OCH_2CH_3$) is the carbonate ester of carbonic acid and ethanol. It is the second homologue of the symmetric dialkyl carbonates family ROC(O)OR. As dimethyl carbonate, DEC has attracted a lot of attention in both industrial and research fields due to its potential eco-friendliness.[1,2]

Although DEC is industrially produced in several ways, it has been synthesized from costless and renewable resources in the last few years by processes with high conversion levels and which avoid the use of toxic reagents.[3] DEC has been considered a bio-based solvent due to the fact that it could be obtained from the ethanolysis of urea or carbon dioxide.[4–6] The profit of this kind of "green" synthetic procedure is even much bigger if we take into account that CO_2 molecules could be used to produce fuel.[7]

Due to its low toxicity and high biodegradability, DEC is widely used as a solvent in the mid-boiling range, replacing more harmful organic substances,[8] and as a raw material in the polymer industry to produce polycarbonates and urethanes.[9,10] Its high oxygen content and good solubility in fuels place it as a fuel additive, reducing the diesel engine emissions of CO_2 and particulates to the environment.[11,12] Additionally, in the last decades, with the development and massive production of rechargeable batteries, DEC was widely employed as electrolyte for lithium cells.[4] For this reason, it is expected that, if the use of carbonates and the rate of production are maintained, their atmospheric emissions will increase drastically. However, to the best of our knowledge, no studies of the gas-phase photochemistry of DEC have been carried out. In this work, we present the results of the determination of the rate coefficient of DEC with chlorine atoms (used as surrogate of $^{\bullet}OH$

radicals) and its photo-oxidation mechanism, which are both supported by experimental measurements and computational studies.

EXPERIMENTAL

General Information

Diethyl carbonate (98%, Sigma Aldrich), ethyl formate (97%, Riedel-deHaën), and formic acid (90%, Dorwil) were used as purchased, while ethyl acetate (Sintorgan) was distilled and stored in molecular sieves prior to use.

Commercially available oxygen (4.8, AGA), nitrogen (4.8, AGA), and carbon monoxide (2.0, Praxair) were used as received. Chlorine (>98% purity) was synthesized by direct reaction between HCl and $KMnO_4$ at inert atmosphere and further distilled, while NO_2 was synthesized by the thermal decomposition of $Pb(NO_3)_2$ in the presence of oxygen and further distilled.

Procedures

Gaseous samples were manipulated using a glass vacuum line equipped with two different capacitance pressure gauges (0 to 760 Torr, MKS Baratron and 0 to 70 mbar, Bell and Howell).

Typical experiments were carried out as follows: a gas-phase mixture of DEC and Cl_2 were prepared in a 5 L previously evacuated glass reactor. Then, either N_2 (for the determination of rate coefficients) or O_2 and NO_2 (for photo-oxidation experiments) were added to reach atmospheric pressure. Finally, a fraction of the gas mixture was transferred to the thermostated infrared glass cell and the photolysis was carried out using two black

lamps. The reaction progress was followed using a Fourier Transform Infrared Spectrometer (Bruker IFS-28) following the temporal variation of reactants and products. All spectra were recorded in the range of 500 to 4000 cm^{-1} with a resolution of 2 cm^{-1}. Control experiments were performed in darkness in order to check for possible heterogeneous reactions.

The kinetics of DEC with chlorine atoms were obtained using the relative method, which employs a reference compound with a well-known rate coefficient and presents no complications such as unwanted secondary reactions.[13] Ethyl acetate (EAc) and ethyl formate (EFor) were used as reference compounds and the results were plotted using Equation 1.

$$\ln\left(\frac{[DEC]_0}{[DEC]_t}\right) - k_{wall} \times t = \frac{k_{DEC}}{k_{reference}} \ln\left(\frac{[reference]_0}{[reference]_t}\right) \quad \text{Eq. 1}$$

The terms $[DEC]_0$, $[DEC]_t$, $[reference]_0$ and $[reference]_t$ represent the concentrations of DEC and reference compound before and after the irradiation time t, respectively. The rate coefficients k_{DEC} and $k_{reference}$ correspond to the reactions of chlorine atoms with DEC and with the reference compound, respectively. A linear fit of the $\ln([DEC]_0/[DEC]_t)$ *vs.* $\ln([reference]_0/[reference]_t)$ gives the slope corresponding to the ratio $k_{DEC}/k_{reference}$. The k_{wall} value (which accounts for overall non-photolytic processes) in typical experiments was 9×10^{-5} s^{-1}.

In order to identify the new products observed as reaction products, their infrared spectrum was calculated using Density Functional Theory with the B3LYP/6-311+G(d,p) basis set and Gaussian09 Program. Frequencies were corrected according to Equation 2 to account for the anharmonicity of the molecule.[14]

$$\nu_{exp}/\nu_{calc} = 1.0 - 0.00001356\ \nu_{calc} \quad \text{Eq. 2}$$

The symbols ν_{exp} and ν_{calc} correspond to the experimental and calculated wavenumbers, respectively.

RESULTS AND DISCUSSIONS

The rate coefficients for the reaction of DEC with chlorine atoms at 298 K (Reaction 1) relative to the reaction of EAc and EFor with chlorine atoms (Reactions 2 and 3) were derived from the slope of the linear plot of $\ln([DEC]_0/[DEC]_t)$ *vs.* $\ln([reference]_0/[reference]_t)$ as showed in Figure 1.

$CH_3CH_2OC(O)OCH_2CH_3 + Cl^{\bullet} \rightarrow$ Products (1)

$CH_3C(O)OCH_2CH_3 + Cl^{\bullet} \rightarrow$ Products (2)

$CH_3CH_2OC(O)H + Cl^{\bullet} \rightarrow$ Products (3)

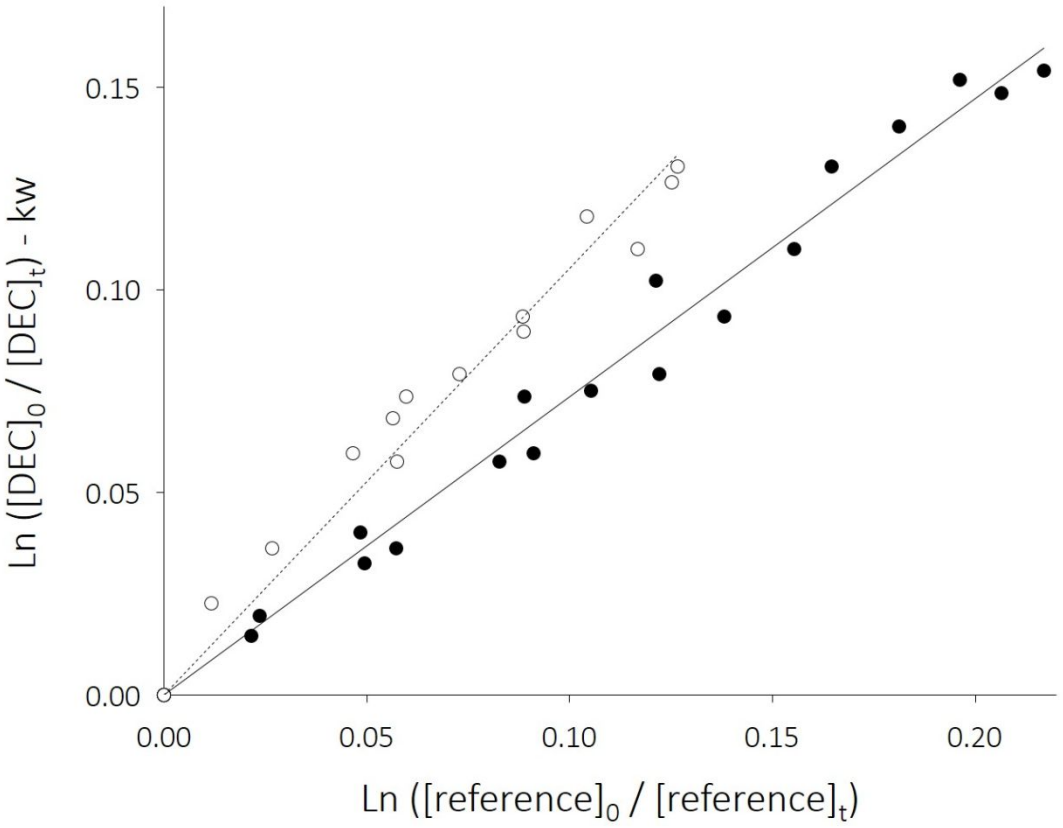

Figure 1. Kinetic data (total pressure 1000 mbar at 298 K) for the reaction of DEC with chlorine atoms relative to EAc (solid circles) and EFor (open circles).

The following slopes, which represent $k_{DEC}/k_{reference}$, were obtained from the plot presented in Figure 1: $k_{DEC}/k_{EAc} = 0.74$ and $k_{DEC}/k_{EFor} = 1.05$. Using the rate coefficient for EAc (1.37×10^{-11} cm^3 molec^{-1} s^{-1})[15] and for EFor (9.92×10^{-11} cm^3 molec^{-1} s^{-1}), available in bibliography,[16] values of 1.01×10^{-11} cm^3 molec^{-1} s^{-1} and 1.04×10^{-11} cm^3 molec^{-1} s^{-1} for k_{DEC} were obtained, respectively. According to the errors derived from the linear fit of our experimental data (5%) and those informed for the rate constants of reference compounds (15% for EAc and 20% for EFor),[15,16] the error rate is estimated at around 20-25%.

Structure-Activity Relationship

The Structure-Activity Relationship (SAR) method was used to corroborate the experimental data. This method, widely used,[17,18] allows the calculation of the rate coefficients of organic molecules based on the estimation of methyl, methylene, and methine group rate constants (k_{prim}, k_{sec}, and k_{tert}, respectively) and parameters (F) associated to the functional groups bonded to each one. The values available in bibliography for these mathematical terms are: $k_{prim} = 3.32 \times 10^{-11}$ cm^3 molecule^{-1} s^{-1}, $k_{sec} = 8.34 \times 10^{-11}$ cm^3 molecule^{-1} s^{-1}, $F(\text{-CH}_3) = 1.00$, $F(\text{-CH}_2\text{-}) = 0.79$, and $F(\text{-CH}_2\text{OC(O)}) = 0.075$.[19] Value for $F(\text{-OC(O)O}) = 0.035$ was derived from the attack of chlorine atoms on dimethyl carbonate, according to the experimental rate coefficient measured by Bilde *et al.*[20]

Considering the values presented above, the rate coefficient for DEC can be estimated as 1.08×10^{-11} cm^3 molec^{-1} s^{-1}, showing an excellent concordance with the

experimental value obtained in this work. This result also corroborates the value of the *F*(-$CH_2OC(O)$) factor obtained by Vila *et al*. for the study of the gas phase degradation of *n*-butyl formate.[19]

From the SAR method, the relative reactivity trend for each hydrogen atom in the molecule can also be estimated. For instance, two possible attack positions are available at DEC moiety: the abstraction of an H-atom from the -CH_2- groups and the corresponding one to -CH_3 groups, herein named "*via* α" and "*via* β" respectively, according to their position with regards to the carbonate moiety. Using the above parameters, a relative reactivity trend of 54% for *via* α and 46% for *via* β were obtained, which shows that both are competitive *vias*.

Reaction mechanism of photo-oxidation

Photo-oxidation products were identified by infrared spectroscopy. The mixture containing DEC (0.41 mbar), Cl_2 (0.30 mbar), and O_2 (1013 mbar) was photolyzed during 60 minutes and two infrared spectra were obtained: one immediately after the lights are turned off, and another after 18h of darkness to study the stability of the photochemical products. The first trace of Figure 2 shows the infrared spectrum obtained immediately after irradiation, in which signals of remaining DEC were already subtracted ("Products" trace). There are clear signals at 1105, 1775 cm^{-1}, and 667 cm^{-1} (corresponding to HCOOH and CO_2 respectively) and 1005, 1152, 1260, and 1828 cm^{-1} (indicated with an asterisk) whose assignment to products will be discussed in the next paragraphs. The subtraction of the spectra of HCOOH and CO_2 to the first trace leads to Trace "A".

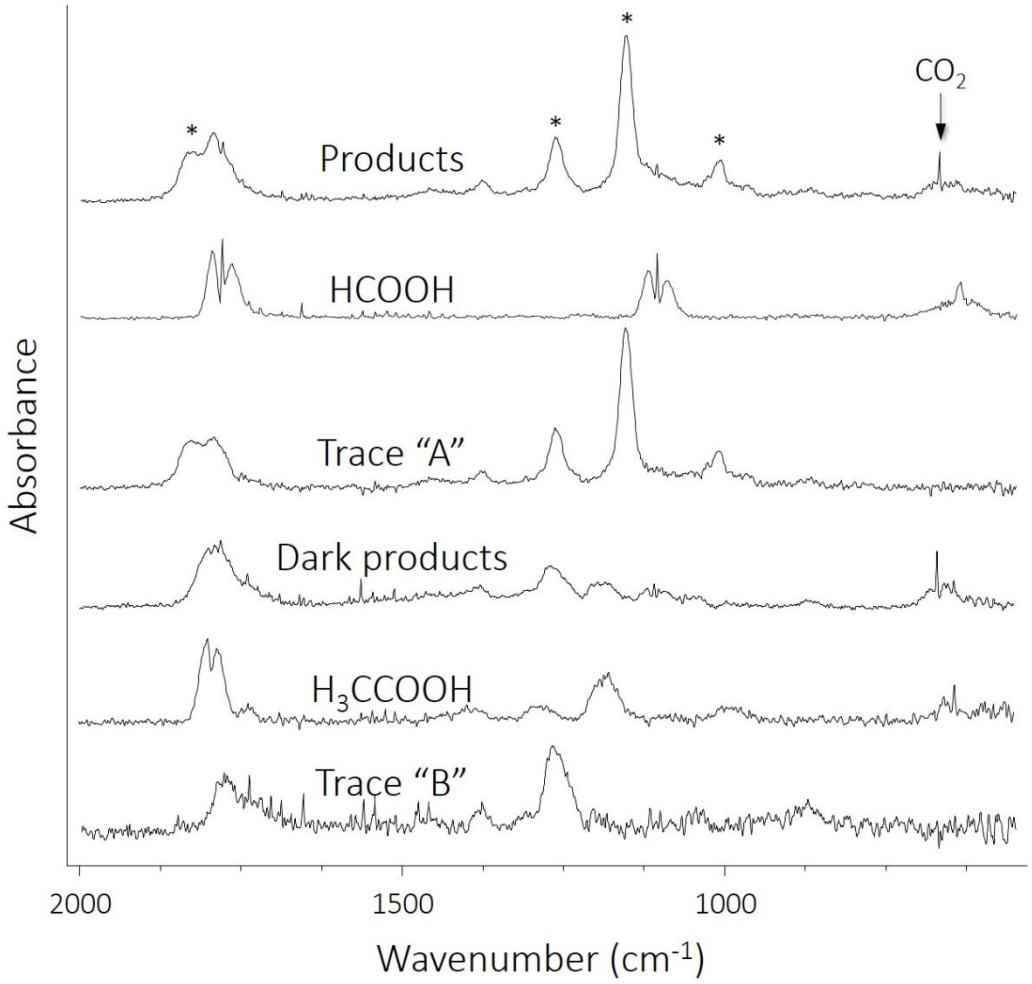

Figure 2. Infrared spectra obtained in the photo-oxidation of DEC. Traces from top to bottom: photo-oxidation products; HCOOH reference; spectrum resulting from the subtraction of HCOOH and CO_2 to the first trace (Trace "A"); dark products; H_3CCOOH reference; spectrum resulting from the subtraction of HCOOH, H_3CCOOH, and CO_2 to Trace "A" (Trace "B").

The fourth trace, "Dark products", shows the spectrum of the irradiated sample after the dark period (unreacted DEC had already been subtracted). As can be seen, in addition to the presence of CO_2 and HCOOH, there were signals of H_3CCOOH indicating its formation

during darkness, while the absorbance of the peaks marked with asterisks in the first trace decreases. The subtraction of the identified products leads to Trace "B".

According to the reaction mechanisms reported for carbo-oxigenated compounds with similar structures to DEC,[20-22] the formation of $CH_3CH_2OC(O)OC(O)CH_3$, $CH_3CH_2OC(O)OCHO$, and $CH_3CH_2OC(O)OCH_2CHO$ as stable photo-degradation products is possible. Using Density Functional Theory, spectra of those species were calculated and compared to our experimental data. The results are presented in Figure 3. A comparison of the theoretical spectrum of $CH_3CH_2OC(O)OCH_2CHO$ with Trace "B" (taken from Figure 2) shows a good agreement, indicating the correspondence of the experimental product to this product. Finally, the subtraction of Trace "B" to Trace "A" leads to the spectrum of a new unstable product that disappears during the dark period (Trace "C"). This product was assigned to $CH_3CH_2OC(O)OC(O)CH_3$, taking into account the agreement between the experimental and calculated infrared spectra showed in the last trace of Figure 3.

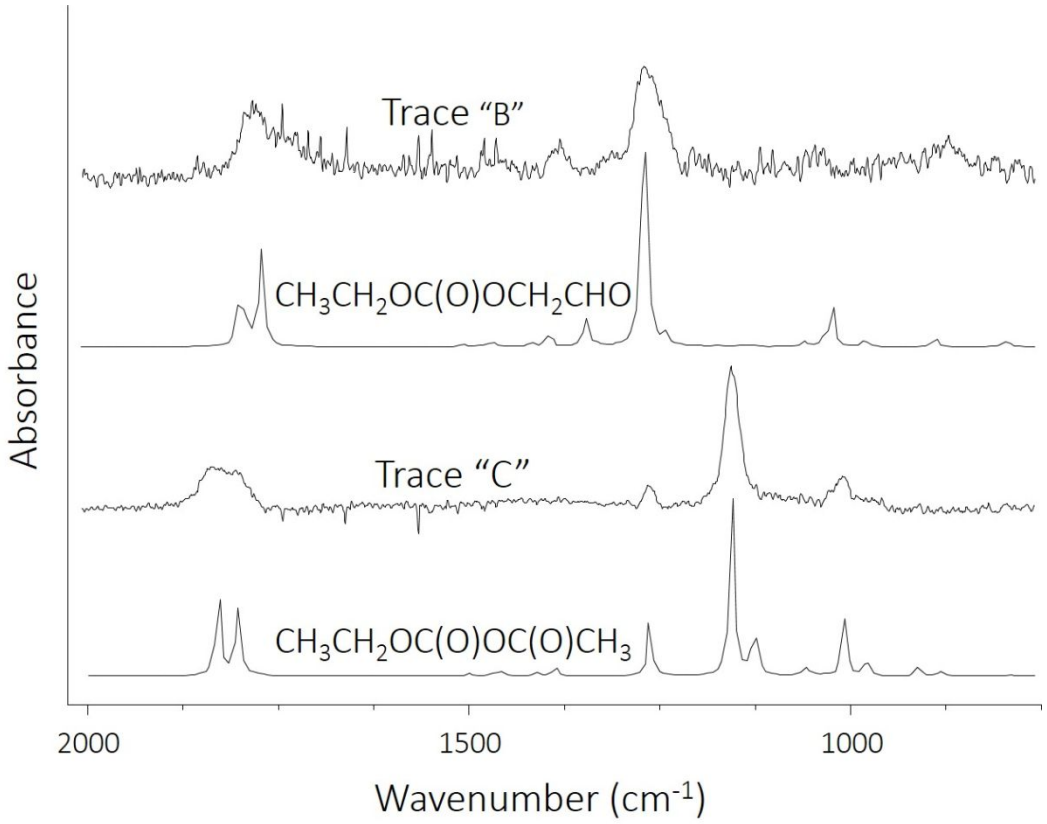

Figure 3. Infrared spectra obtained in the photo-oxidation of DEC. Traces from top to bottom: Trace "B" taken from Figure 2; theoretical spectrum of $CH_3CH_2OC(O)OCH_2C(O)H$; spectrum resulting from the subtraction of Trace "B" to Trace "A" (Trace "C"); theoretical spectrum of $CH_3CH_2OC(O)OCH_2CH_3$.

The formation of the unstable $CH_3CH_2OC(O)OC(O)CH_3$ was also proved by the appearance of acetic acid during the dark period, which comes from the heterogeneous degradation of the $-OC(O)CH_3$ fragment. Similarly, the appearance of formic acid during photolysis was attributed to the formation of a more unstable anhydride containing the –C(O)OC(O)H group, which decomposes completely during photo-oxidation: $CH_3CH_2OC(O)OCHO$.

Photo-oxidation experiments in the presence of NO_2 were also performed. Mixture of DEC (0.41 mbar), Cl_2 (0.30 mbar), NO_2 (0.40 mbar), and O_2 (1013 mbar) was photolyzed and analyzed. The most remarkable result is the appearance of a set of signals at 794, 1163, 1741, and 1842 cm^{-1}, corresponding to the characteristic peaks of peroxy acetyl nitrate (PAN, $CH_3C(O)OONO_2$).[23] This result suggests the formation of the $CH_3C(O)^{\bullet}$ radical during the photo-oxidation, which leads the formation of PAN according to reactions 4 and 5.

$$CH_3C(O)^{\bullet} + O_2 \rightarrow CH_3C(O)OO^{\bullet} \quad (4)$$

$$CH_3C(O)OO^{\bullet} + NO_2 \rightarrow CH_3C(O)OONO_2 \quad (5)$$

Finally, a set of experiments varying the oxygen partial pressure (from 70 to 1013 mbar) inside the photo-reactor were performed. Spectra were recorded at 60 minutes of photolysis and after 18 hours in darkness. The quantification of carbon monoxide, carbon dioxide, formic acid, and acetic acid was performed using their corresponding calibration curve at the same experimental conditions used in the experimental set-up. $CH_3CH_2OC(O)OC(O)CH_3$ and $CH_3CH_2OC(O)OCHO$ were quantified from their decomposition product (*i.e.* acetic and formic acid, respectively) after the dark period to ensure their complete decomposition. Formaldehyde was quantified from its photo-oxidation product (CO) taking into account the rate coefficient of reaction between chlorine atoms and CH_2O (7.3×10^{-11} cm^3 $molecule^{-1}$ s^{-1}) is higher to the rate coefficient of reaction with DEC (1.02×10^{-11} cm^3 $molecule^{-1}$ s^{-1}). Figure 4 shows the percentage of products relative to the disappearance of DEC, determined as a function of the oxygen partial pressure. As can be seen, when O_2 partial pressure increases, the concentrations of CO and CO_2 decrease while $CH_3CH_2OC(O)OC(O)CH_3$ increases. It is interesting to note that the

concentration of $CH_3CH_2OC(O)OCHO$ does not change in the analyzed range of O_2 partial pressures. The high percentage of CO_2 formation is a consequence that it is formed in several ways, as will be discussed later. PAN quantification (not showed in the plot) was also performed in the photo-oxidation in the presence of NO_2 at 1013 mbar total pressure, leading to a percentage formation of 25%.

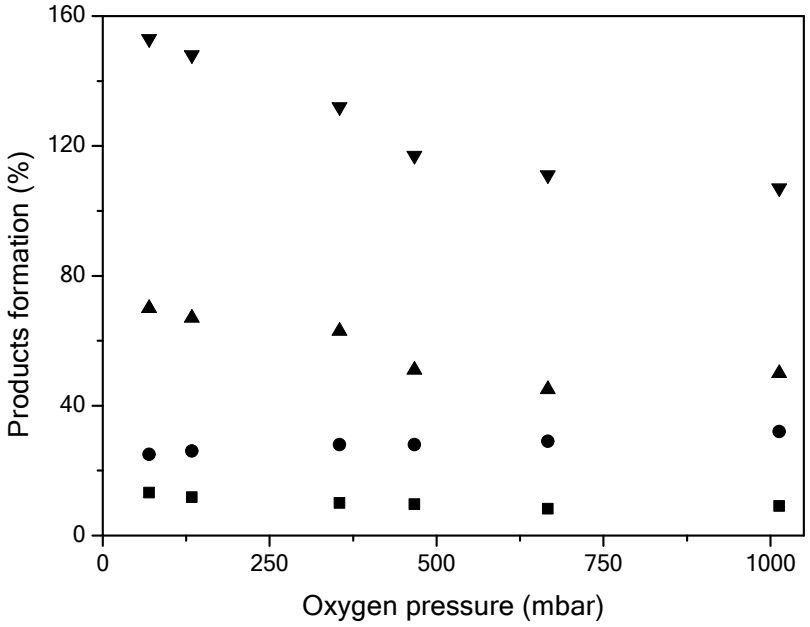

Figure 4. Products percentages relative to DEC disappearance as a function of O_2 pressure (70 − 1013 mbar): CO_2 (down triangles), H_2CO (upper triangles), $CH_3CH_2OC(O)OC(O)CH_3$ (solid circles), and $CH_3CH_2OC(O)OCHO$ (solid squares).

According to the experimental results, the following photo-oxidation mechanism was postulated (Scheme 1):

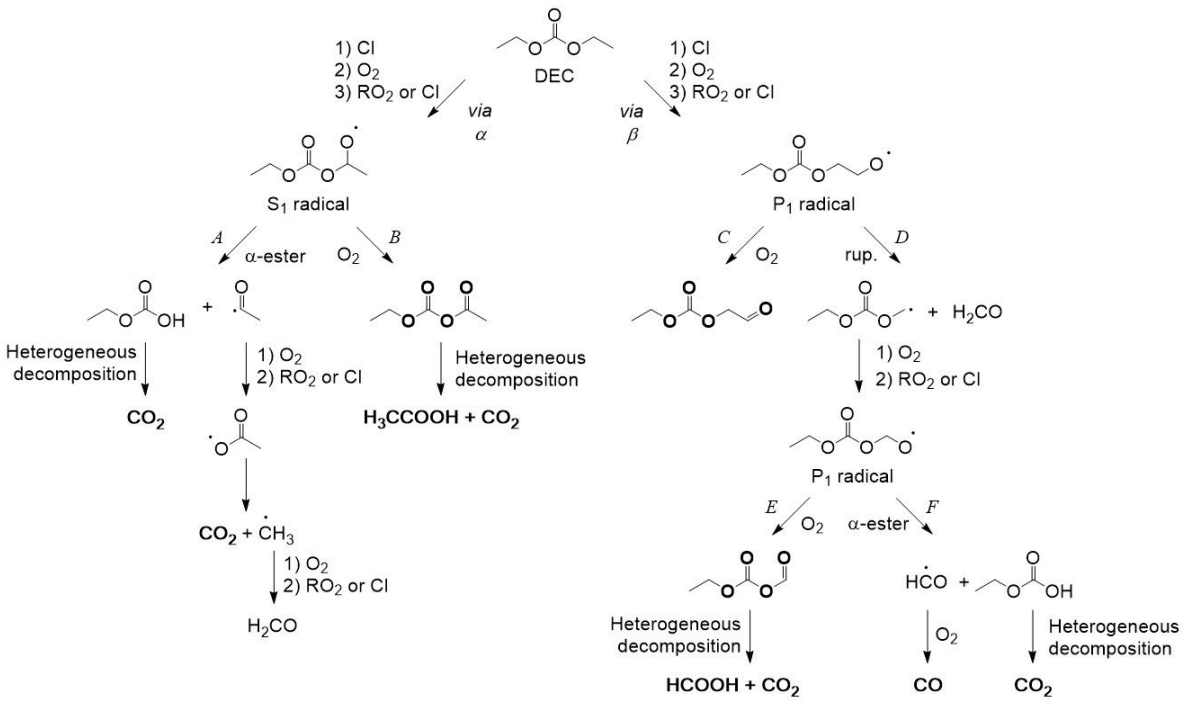

Scheme 1. Proposed mechanism for the Cl-atoms initiated oxidation of DEC.

Essentially, chlorine atoms attack DEC at both possible positions (-CH_3 and -CH_2- groups) abstracting an H-atom from each one. Both resulting radicals react with O_2 to form the corresponding peroxy radical, which subsequently reacts either with chlorine atoms or another peroxy radical, leading to the secondary radical S_1 ($CH_3CH_2OC(O)OCHO^{\bullet}CH_3$) and the primary radical P_1 ($CH_3CH_2OC(O)OCH_2CH_2O^{\bullet}$) radicals (*via* α and β, respectively).

It is well known that the main path for radicals with a chemical structure similar to S_1 (R-C(O)$OCH_2O^{\bullet}$) is the α-ester rearrangement[24,25] and the reaction with O_2 and their relative importance are dependent of the oxygen pressure in the system.[26] This agrees with the large amount of $CH_3CH_2OC(O)OC(O)CH_3$ formed in the experiments carried out at higher oxygen pressures (Figure 4), as it is depicted in Scheme 1, Path *B*.

On the other hand, the α-ester rearrangement of S_1 radical leads finally to the formation of CO_2 (via the degradation of unstable CH_3CH_2OCOOH and the $CH_3C(O)O^\bullet$ radical), formaldehyde, and additionally PAN when the photolysis is carried out in the presence of nitrogen dioxide. It is important to note that monoethyl carbonic acid ester (CH_3CH_2OCOOH) was not observed in our system due to its extreme instability and decomposed to an equimolar amount of CO_2.[27]

For the P_1 radical ($CH_3CH_2OC(O)OCH_2CH_2O^\bullet$), the reaction with O_2 and rupture are both available degradation paths. The first one leads to the formation of $CH_3CH_2OC(O)OCH_2CHO$ (Scheme 1, Path *C*), while the second leads to the formation of $CH_3CH_2OC(O)OCH_2^\bullet$ and formaldehyde (Scheme 1, Path *D*).

The $CH_3CH_2OC(O)OCH_2^\bullet$ radical formed follows the same sequence previously mentioned for the primary step, leading to the formation of the $CH_3CH_2OC(O)OCH_2O^\bullet$ radical, named P_2 radical. At this point, two paths are available as discussed for the S_1 radical above: α-ester rearrangement and reaction with O_2.[21,24] The reaction with O_2 (Scheme 1, Path *E*) was corroborated by the formation of $CH_3CH_2OC(O)OCHO$. The α-ester rearrangement was inferred considering that it is a competitive main path for the similar $CH_3CH_2C(O)OCH_2O^\bullet$ radical.[28] According to this, the final products of path *F* are CO_2 (originated from the decomposition of the unstable CH_3CH_2OCOOH) and CO.

From the previous analysis and the percentages of product formation presented in Figure 4, the percentages of attack of the chlorine atom on the methyl group and methylene group were determined. The *via* α percentage can be determined from the sum of $CH_3CH_2OC(O)OC(O)CH_3$ (32%) and PAN (25%). The percentage of *via* α (57%) was

determined according to these values and inferred the values for *via β* (43%) in agreement with those obtained from the SAR method (54% and 46%, respectively).

Computational Studies

Quantum chemical calculations using the DFT level of theory (B3LYP/6-311+G(d,p) functional, Gaussian09 Program system)[29] have been carried out in order to investigate the main reaction paths of DEC. Full geometry optimizations were performed, followed by harmonic frequency calculations at the same level of theory, which also allowed the characterization of the nature of the stationary points.[30,31]

As depicted above in the mechanism reaction showed in Scheme 1, we suggest two main ways (*vias α* and *β*). Besides the fact that the H abstraction from DEC by Cl are quite energetically similar for both positions, calculations show that, after oxidation, the resulting S_1 radical is about 39 kJmol^{-1} lower in energy than the P_1 radical.

Figure 5 shows the energy corresponding to the main path reactions of S_1 and P_1 radicals. As can be seen, the formation of unstable $CH_3CH_2OC(O)OH$ from *α*-ester rearrangement of S_1 (path *A,* left panel) is favored over the formation of the stable $CH_3CH_2OC(O)OC(O)CH_3$ coming from the reaction between S_1 and O_2 (path *B,* right panel). Unraveling the different possibilities to achieve $CH_3CH_2OC(O)OH$, calculation showed that it could be obtained through two possible processes that occur in a concerted but slightly asynchronous manner, with an energy difference of only 2 kJ mol^{-1}. On the other hand, conformational analysis for path *B* allows to identify the conformer that leads to the formation of $CH_3CH_2OC(O)OC(O)CH_3$ through the H atom subtraction with a relative

energy barrier of 108 kJmol^{-1}, which is higher than those which lead to a $CH_3CH_2OC(O)OH$ formation.

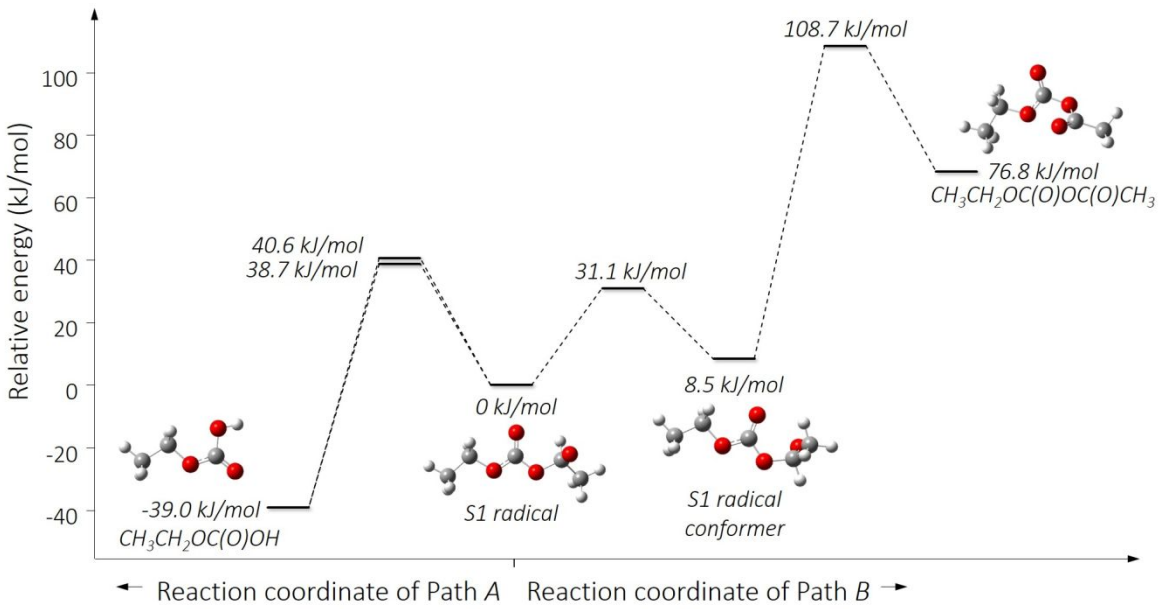

Figure 5. Partial reaction coordinates for S_1 radical: path A (left) and path B (right).

In the same way, reaction paths for P_1 radical (Scheme 1, *via β*) were also analyzed theoretically. Theoretical calculations (Figure 6, left panel) show that either energy activation that leads to $CH_3CH_2OC(O)OCH_2CHO$ from its reaction with molecular oxygen (Scheme 1, Path *C*) or $CH_3CH_2OC(O)OCH_2^{\bullet}$ radical generated by C-C bond fragmentation (Scheme 1, Path *D*) are high enough to explain the low occurrence of these paths. However, a comparison of the activation energy of both paths shows that the formation of $CH_3CH_2OC(O)OCH_2^{\bullet}$ radical and formaldehyde is 62.7 kJmol^{-1} and is favored over the formation of $CH_3CH_2OC(O)OCH_2CHO$.

Computational calculations were also extended to determine the most favorable reaction pathway for the $CH_3CH_2OC(O)OCH_2O^{\bullet}$ radical (P_2) originated from the

$CH_3CH_2OC(O)OCH_2^{\bullet}$ radical. The energy required for both available paths (*E* and *F*), that is for the reaction with O_2, and for the α-ester rearrangement, are very different indicating that path E is favored. Moreover, as it was described above for path *A*, the formation of $CH_3CH_2OC(O)OH$ could be achieved through two possible processes which are, at least, 64 $kJmol^{-1}$ lesser in energy than path *E*.

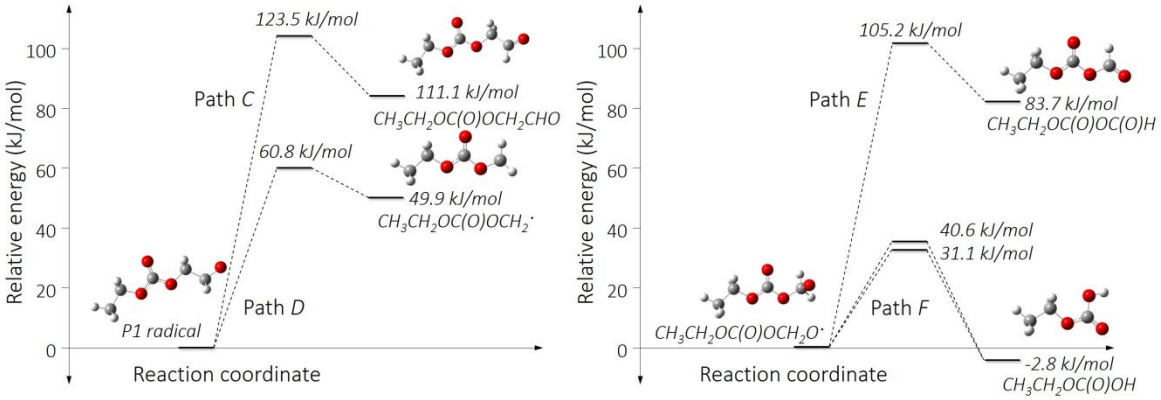

Figure 6. Partial reaction coordinates for P_1 radical: path C and D (left panel) and path E and F (right panel).

CONCLUSIONS

The rate coefficient for DEC with chlorine atoms was determined using the relative method and a mean value of $(1.0 \pm 0.2) \times 10^{-11}$ cm^3 $molecule^{-1}$ s^{-1} was obtained. This value is in good agreement with those calculated using the Structure-Activity Relationship method (1.08×10^{-11} cm^3 $molec^{-1}$ s^{-1}).

The reaction mechanism for the Cl-atoms initiated by photo-oxidation was determined from the products identification and numerical calculations performed for the

main paths reactions. Results show that the chlorine attacks both methyl (43%) and methylene groups (57%), leading to the formation of $CH_3CH_2OC(O)OCHO$, $CH_3CH_2OC(O)OCH_2CHO$, $CH_3CH_2OC(O)OC(O)CH_3$, CH_2O, CO_2, and CO. Theoretical calculations show that decomposition via α-ester rearrangement and reaction with molecular oxygen are competitive atmospheric reaction paths for both $CH_3CH_2OC(O)OCH_2O^{\bullet}CH_3$ and $CH_3CH_2OC(O)OCH_2O^{\bullet}$ radicals, while rupture is the main path for the $CH_3CH_2OC(O)OCH_2CH_2O^{\bullet}$ radical.

ACKNOWLEDGMENTS

Financial support from SECYT-UNC, ANPCYT, and CONICET is gratefully acknowledged. This work used computational resources from CCAD-Universidad Nacional de Córdoba, in particular the Mendieta Cluster, which is part of SNCAD-MinCyT, República Argentina. FEM thanks Gil Michel for English language assistance.

REFERENCES

(1) Pacheco, M. A.; Marshall, C. L. Review of dimethyl carbonate (DMC) manufacture and its characteristics as a fuel additive. *Energy and Fuels* **1997**, *11* (1), 2–29.

(2) Bracco, P.; Domínguez de María, P. In *Bio-Based Solvents*; Jerome, F., Luque, R., Eds.; Wiley, 2017; pp 113–130.

(3) Leino, E.; Mäki-Arvela, P.; Eta, V.; Murzin, D. Y.; Salmi, T.; Mikkola, J.-P. Conventional synthesis methods of short-chain dialkylcarbonates and novel production tecnology via direct route from alcohol and waste CO_2. *Appl. Catal. A Gen.* **2010**, *383* (1–2), 1–13.

(4) Wang, D.; Yang, B.; Zhai, X.; Zhou, L. Synthesis of diethyl carbonate by catalytic alcoholysis of urea. *Fuel Process. Technol.***2007**, *88* (8), 807–812.

(5) Shukla, K.; Srivastava, V. C. Synthesis of organic carbonates from alcoholysis of urea: A review. *Catal. Rev.* **2017**, *59*, 1–43.

(6) Leino, E.; Mäki-Arvela, P.; Eränen, K.; Tenho, M.; Murzin, D. Y.; Salmi, T.; Mikkola, J.-P. Enhanced yields of diethyl carbonate via one-pot synthesis from ethanol, carbon dioxide and butylene oxide over cerium (IV) oxide. *Chem. Eng. J.* **2011**, *176–177*, 124–133.

(7) Zevenhoven, R.; Eloneva, S.; Teir, S. Chemical fixation of CO_2 in carbonates:

Routes to valuable products and long-term storage. *Catal. Today* **2006**, *115* (1–4), 73–79.

(8) Schäffner, B.; Schäffner, F.; Verevkin, S.; Börner, A. Organic carbonates as solvents in synthesis and catalysis. *Chem. Rev.* **2010**, *110*, 4554–4581.

(9) Shaikh, A.-A. G.; Sivaram, S. Organic Carbonates. *Chem. Rev.* **1996**, *96*, 951–976.

(10) Matsumura, S.; Harai, S.; Toshima, K. Lipase-catalyzed polymerization of diethylcarbonate and diol to aliphatic poly(alkylenecarbonate). *Macromol. Chem. Phys.* **2000**, *201* (14), 1632–1639.

(11) Dunn, B. C.; Guenneau, C.; Hilton, S. A.; Pahnke, J.; Eyring, E. M.; Dworzanski, J.; Meuzelaar, H. L. C.; Hu, J. Z.; Solum, M. S.; Pugmire, R. J. Production of diethyl carbonate from ethanol and carbon monoxide over a heterogeneous catalyst. *Energy & Fuels* **2002**, *16*, 177–181.

(12) Shukla, K.; Srivastava, V. C. Diethyl carbonate: critical review of synthesis routes, catalysts used and engineering aspects. *RSC Adv.* **2016**, *6* (39), 32624–32645.

(13) Atkinson, R. Kinetics and mechanisms of the gas-phase reactions of the hydroxyl radical with organic compounds under atmospheric conditions. *Chem. Rev.* **1986**, *86* (1), 69–201.

(14) Yoshida, H.; Takeda, K.; Okamura, J.; Ehara, A.; Matsuura, H. A new approach to vibrational analysis of large molecules by Density Functional Theory: Wavenumber-Linear scaling method. *J. Phys. Chem. A* **2002**, *106*, 3580–3586.

(15) Cuevas, C. A.; Notario, A.; Martínez, E.; Albaladejo, J. Influence of temperature in the kinetics of the gas-phase reactions of a series of acetates with Cl atoms. *Atmos. Environ.* **2005**, *39*, 5091–5099.

(16) Calvert, J. G.; Mellouki, A.; Orlando, J. J.; Pilling, M. J.; Wallington, T. J. *Mechanisms of Atmospheric Oxidation of the Oxygenates*; Oxford University Press, 2011.

(17) Atkinson, R. Structure-activity relationship for the estimation of rate constants for the gas-phase reactions of hydroxyl radicals with organic compounds. *Int. J. Chem. Kinet.* **1987**, *19* (9), 799–828.

(18) Kwok, E. S. C.; Atkinson, R. Estimation of hydroxyl radical reaction rate constants for gas-phase organic compounds using a structure-reactivity relationship: an update. *Atmos. Environ.* **1995**, *29* (14), 1685–1695.

(19) Vila, J. A.; Argüello, G. A.; Malanca, F. E. Atmospheric degradation of n-butyl formate in the presence of O_2 and NO_2. *J. Photochem. Photobiol. A Chem.***2018**, *361*, 105–111.

(20) Bilde, M.; Mogelberg, T. E.; Sehested, J.; Nielsen, O. J.; Wallington, T. J.; Hurley, M. D.; Japar, S. M.; Dill, M.; Orkin, V. L.; Buckley, T. J.; Huie, R. E.; Kurylo, M. J. Atmospheric chemistry of dimethyl carbonate: reaction with OH radicals, UV spectra of $CH_3OC(O)OCH_2$ and $CH_3OC(O)OCH_2O_2$ radicals, reactions of $CH_3OC(O)OCH_2O_2$ with NO and NO_2, and fate of $CH_3OC(O)OCH_2O$ radicals. *J. Phys. Chem. A.* **1997**, *101*, 3514–3525.

(21) Cavalli, F.; Barnes, I.; Becker, K. H.; Wallington, T. J. Atmospheric oxidation mechanism of methyl propionate. *J. Phys. Chem. A* **2000**, *104* (48), 11310–11317.

(22) Christensen, L. K.; Ball, J. C.; Wallington, T. J. Atmospheric oxidation mechanism of methyl acetate. *J. Phys. Chem. A*. **2000**, *104* (2), 345-351.

(23) Allen, G.; Remedios, J. J.; Smith, K. M. Low temperature mid-infrared cross-sections for peroxyacetyl nitrate (PAN) vapour. *Atmos. Chem. Phys.* **2005**, *5*, 3153–

3158.
(24) Orlando, J. J.; Tyndall, G. S.; Wallington, T. J. The atmospheric chemistry of alkoxy radicals. *Chem. Rev.* **2003**, *103* (12), 4657–4689.
(25) Rayez, M. T.; Picquet-Varrault, B.; Caralp, F.; Rayez, J. C. $CH_3C(O)OCH(O^{\cdot})CH_3$ alkoxy radical derived from ethyl acetate: Novel rearrangement confirmed by computational chemistry. *Phys. Chem. Chem. Phys.* **2002**, *4* (23), 5789–5794.
(26) Tyndall, G. S.; Pimentel, A. S.; Orlando, J. J. Temperature dependence of the alpha-ester rearrangement reaction. *J. Phys. Chem. A.* **2004**, *108* (33), 6850–6856.
(27) Bernard, J.; Köck, E. M.; Huber, R. G.; Liedl, K. R.; Call, L.; Schlögl, R.; Grothe, H.; Loerting, T. Carbonic acid monoethyl ester as a pure solid and its conformational isomerism in the gas-phase. *RSC Adv.* **2017**, *7*, 22222–22233.
(28) Andersen V. F., Berhanu T. A., Nilsson E. J., Jørgensen S., Nielsen O. J., Wallington T. J., Johnson M. S. Atmospheric chemistry of two biodiesel model compounds: methyl propionate and ethyl acetate. *J. Phys. Chem. A.* **2011**, *115*, 8906 - 8919.
(29) Frisch, M. J.; Trucks, G. W.; Schlegel, H. B.; Scuseria, G. E.; Robb, M. A.; Cheeseman, J. R.; Scalmani, G.; Barone, V.; Petersson, G. A.; Nakatsuji, H.; *et al Gaussian, Inc., Wallingford CT* **2009**.
(30) Pepino, A. J.; Peláez, W. J.; Faillace, M. S.; Ceballos, N. M.; Moyano, E. L.; Argüello, G. A. (S)-5-Benzyl- and 5-benzylidene-imidazo-4-one derivatives synthesized and studied for an understanding of their thermal reactivity. *RSC Adv.* **2014**, *4*, 60092–60101.
(31) Peláez, W. J.; Pepino, A. J.; Argüello, G. A.; Pinho E Melo, T. M. V. D. 1-Methyl-5-(trifluoromethyl)azafulvenium methide, an intermediate that undergoes reaction through "unusual" cis-exo-1,3- and trans-exo-1,7-Cycloadditions. *European J. Org. Chem.* **2014**, 2933–2941.

TOC GRAPHIC